



Instrument Noise characterization and the Allan/M-sample variance

Jonathan Mittaz

National Physical Laboratory/University of Reading

16/02/16



FIDUCEO has received funding from the European Union's Horizon 2020 Programme for Research and Innovation, under Grant Agreement no. 638822

Instrument Noise characterization and the Allan/M-sample variance

1 Contents

2	Introduction	2
2.1	Scope.....	2
2.2	Version Control	2
2.3	Applicable and Reference Documents.....	2
2.4	Glossary.....	2
3	Variance estimation	3
4	Noise estimation from satellite data	4
4.1	Simulated datasets at full resolution	4
4.1.1	Allan variance and different noise spectra	4
4.1.2	Determining the noise spectrum	6
4.2	Simulated data with gaps and with digitisation.....	8
4.2.1	Gaps in the data	8
4.2.2	Effect of digitisation	10
4.3	Analysis of data from the AVHRR.....	10
4.3.1	NOAA-14	11
4.3.2	TIROS-N	12
4.3.3	NOAA-07	17
4.3.4	Correlations between the noise and ICT radiance.....	18

Instrument Noise characterization and the Allan/M-sample variance

2 Introduction

This document describes different techniques for analysing and determining the noise characteristics of a sensor flown on-board a heritage instrument such as the Advanced Very High Resolution Radiometer (AVHRR). It will be shown that there are potential problems involved in taking a simplistic approach to such analyses and by using techniques such as the Allan variance issues such as non-stationary trends can be significantly reduced without requiring prior knowledge of the underlying trend behaviour. The issue of different noise types (white, pink, red, blue and violet) is also discussed by using the Allan variance together with the M-sample variance as a discriminator. It is shown that to use the B_1 bias estimator account has to be taken of any strong digitisation of the input data. Finally, real satellite data from the AVHRR is used as an example of the proposed use of both the Allan variance together with the detection of the underlying noise spectrum.

2.1 Scope

Determining the underlying noise characteristics from the FIDUCEO Level 1 instruments is central to being able to provide both GUM like uncertainties as well as providing input into Monte-Carlo schemes. This document provides statistics methods to both determine estimates of the underlying noise as well as estimates of the noise power spectrum.

2.2 Version Control

Version	Reason	Reviewer	Date of Issue
1.a	Original draft		
1.b			
1.c			

2.3 Applicable and Reference Documents

[1] Allan, D, 1966, Statistics of Atomic Frequency Standards, Proceedings of IEEE, 54, 211-230

[2] Barnes, J.A. & Allan, D., 1990, Variances Based on Data with Dead Time Between the Measurements, NIST Technical Note 1318

[3] Tian, M, Zou, X. & Weng, F., 2015, Use of Allan deviation for characterising satellite microwave sounder noise equivalent differential temperature (NEDT), IEEE Geoscience and Remote Sensing Letters, 12, 2477 – 2480 doi: [10.1109/LGRS.2015.2485945](https://doi.org/10.1109/LGRS.2015.2485945)

2.4 Glossary

Instrument Noise characterization and the Allan/M-sample variance

3 Variance estimation

All measurements include a noise component that should be characterised in a manner that is independent of other on-going process and ideally provide extra information on the underlying behaviour of the noise itself. There are a number of different algorithms that can be used to estimate the standard deviation/noise of a given dataset. The standard form for the variance of the data is given by

$$S^2 = \frac{1}{N-1} \sum_{n=1}^N (y_n - \langle y \rangle)^2$$

where

$$\langle y \rangle = \frac{1}{N} \sum_{n=1}^N y_n$$

Other ways of estimating the variance exist. One of these is the so-called “Allan variance” or “two sample variance” which is a particular form of the M-sample variance [1]. The M-sample variance is defined as

$$S_n^2(M, T, t) = \frac{1}{M-1} \left\{ \sum_{i=0}^{M-1} y_i^2 - \frac{1}{M} \left[\sum_{i=0}^{M-1} y_i \right]^2 \right\}$$

with the associated total variance as

$$S^2(M, T, t) = \langle S_y^2(M, T, t) \rangle$$

where the time-length of each observation is t , the time between observations is T and M is the number of samples used in each step.

The Allan variance is a particular form of the M-sample variance such that

$$S_{Allan}^2(t) = \langle S_y^2(2, t, t) \rangle$$

which can be conveniently written as

$$S_{Allan}^2(t) = \frac{1}{2} \langle (y_{n+1} - y_n)^2 \rangle$$

This last version of the equation highlights one of the strengths of the Allan variance. In the case where the underlying mean value of the observations varies over time (as can be the case with observing internal calibration targets for example) the Allan variance will not be significantly impacted as it is related to the average of the difference between adjacent measurements that occur on much shorter timescales than any longer term trends.

Instrument Noise characterization and the Allan/M-sample variance

Using the general form of the M-sample variance can also help determine the underlying noise spectral slope μ . This can then help interpret the data and determine the source of noise in the system. This is because physical processes can generate different noise characteristics with different noise spectra. We can use the M-sample variance because the noise spectral slope is related to so called Bias functions including

$$B_1(N, r, m) = \frac{\langle S_y^2(N, T, t) \rangle}{\langle S_y^2(2, T, t) \rangle}$$

where $r = T / t$ and B is a function of μ through the noise characteristics of the y's. Other bias functions exist where changes in r are used (B_2) and where the impact of variable dead time between observations is taken into account (B_3) [2]. For the purposes of satellite data where the observation time τ and r is generally a constant B_1 is likely to be the most useful of the bias functions.

4 Noise estimation from satellite data

Here we are considering how to estimate noise sources from Earth observation satellite data where it is common practice to estimate the instrument noise using simple statistics such as the mean and variance of sections of data. As pointed out by [3], however, a simplistic approach can provide erroneous results, especially if the data used to estimate the noise contains underlying non-stationary processes such as observations of the internal calibration targets that vary in temperature around an orbit. To determine the best way of determining variance and noise spectra we start by looking at simulated data.

4.1 Simulated datasets at full resolution

To begin to investigate the different properties of variance estimation we have created simulated data that are at full resolution with no gaps present and with full floating point values. The top panel of Figure 1 shows a simulated example where white noise (noise taken from a normal probability distribution) with a standard deviation of 0.5 has been added to a sinusoidal variation. The signal and noise values are consistent with typical variations seen for the 11 μ m channel for observation of the internal calibration target of the AVHRR. The middle panel shows the normal standard deviations derived for segments of data taken around the 'orbit' where the impact of the non-stationary behaviour on the standard deviation can be seen. Finally, the lower panel shows the Allan variance using the same data where the impact of the sinusoidal variation is absent from the estimated variance. This shows the usefulness of the Allan variance for noise estimation particularly where the mean of the data is time variable.

4.1.1 Allan variance and different noise spectra

To investigate this further we have also simulated datasets that have different noise spectra. We have chosen five different forms of noise. First is white noise that is a random noise with a constant power density spectrum. Second is pink noise or 1/f noise where the power density spectrum is inversely proportional to the frequency. Third is red noise, the sort of noise produced by Brownian motion and is sometimes called random walk noise that has a spectrum of order $1 / f^2$. Fourth is blue noise where the noise is proportional to frequency. Finally there is violet noise which has a spectrum of order frequency squared. Some of these noise types can be related to different physical processes. For example, pink noise

Instrument Noise characterization and the Allan/M-sample variance

is often seen in electronics and can arise from fluctuating configurations of defects in metals or fluctuating occupancies of traps in semiconductors. Figure 2 shows examples of time series created with some of these different noise spectra for a constant input signal. Figure 3 shows both the normal standard deviation and the Allan standard deviations for all five cases and shows that for different noise spectra the behaviour between the two methods is different. The standard method of calculating the standard deviation has severe problems with the red noise case but seems to work slightly better for the other noise spectra. It must be kept in mind, however, that we have used a constant input source for this example and the standard method of calculating the standard deviation is much more sensitive to variations in the mean than the Allan variance. This plot also highlights the importance of knowing the underlying noise spectrum for a given case in order to understand the relationship between the variance and the underlying input noise value. To accurately simulate the noise within a Monte-Carlo framework for example one should use an estimate of the input noise spectrum rather than a single number if the noise spectrum is non-white.

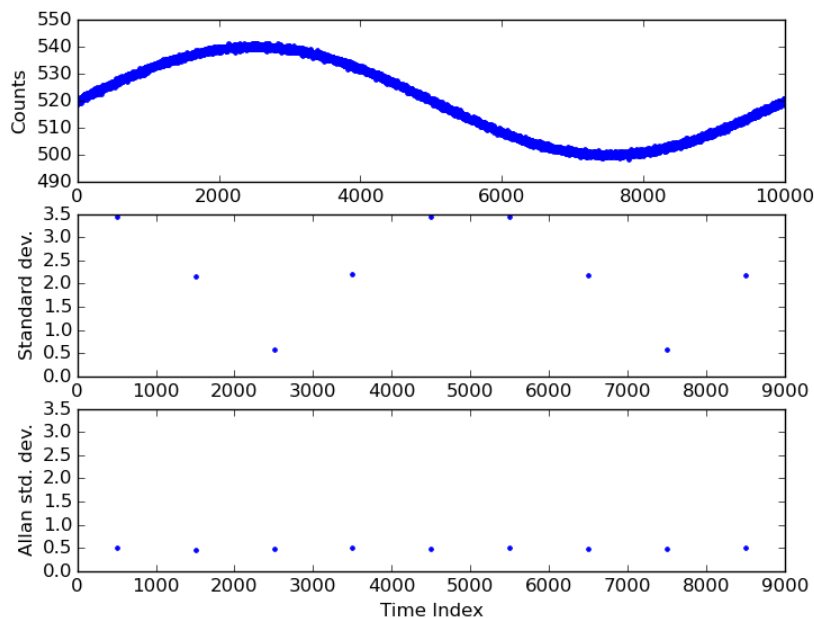


Figure 1 Simulated data for a variable signal together with the standard deviations calculated over 1000 point segments and the Allan standard deviation calculated over the same segments. While the normal standard deviation shows variation due to the non-stationary nature of the input data, the Allan standard deviation is very close to the input noise value of 0.5 counts.

Instrument Noise characterization and the Allan/M-sample variance

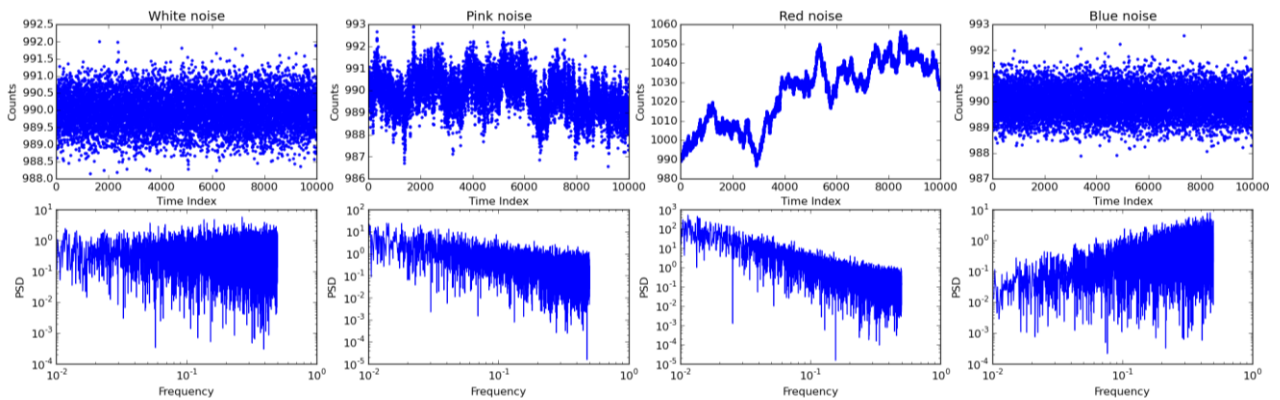


Figure 2 Simulated data with three different noise spectra (white, pink, red and blue). The top four panels show the time series and the lower four panels show the noise frequency spectra. The input standard deviation to all noise generators was 0.5 counts.

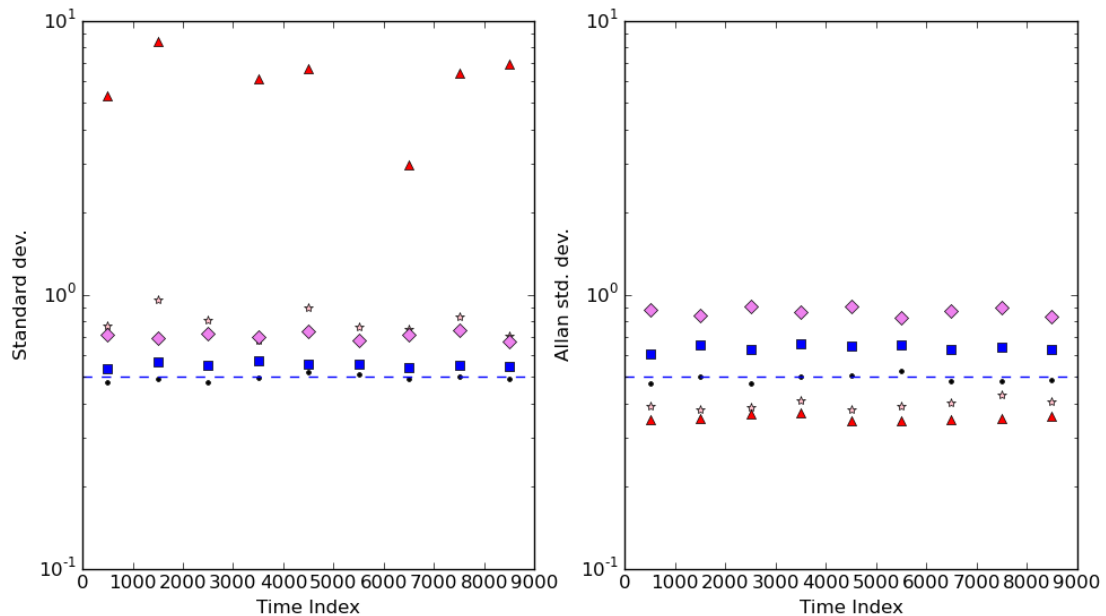


Figure 3 Left hand panel shows the standard deviation from time series from simulated data with a constant input noise using five different noise spectra (white (dot), pink (star), red (triangle), blue (square) and violet (diamond)) with an input noise of 0.5 counts. The normal way of calculating the standard deviation is particularly biased for the red (random-walk) noise spectrum. The right hand panel shows the Allan standard deviation for the same data that has less of a problem with the red (random-walk) noise spectrum but shows slightly larger deviations from the input (0.5 value).

4.1.2 Determining the noise spectrum

We have shown that using the Allan variance under different circumstances (variable signal, different noise spectra) works better than the standard way of calculating variance. The M-sample variance coupled with the Allan variance can also distinguish between different noise spectra [1]. One way to do this is to look at the variation of $B_1(M)$ as a function of M. An example is shown in Figure 4 where the values of $B_1(M)$ for the five different noise cases (white, pink, red, blue and violet) are shown for all 10000 simulated samples.

Instrument Noise characterization and the Allan/M-sample variance

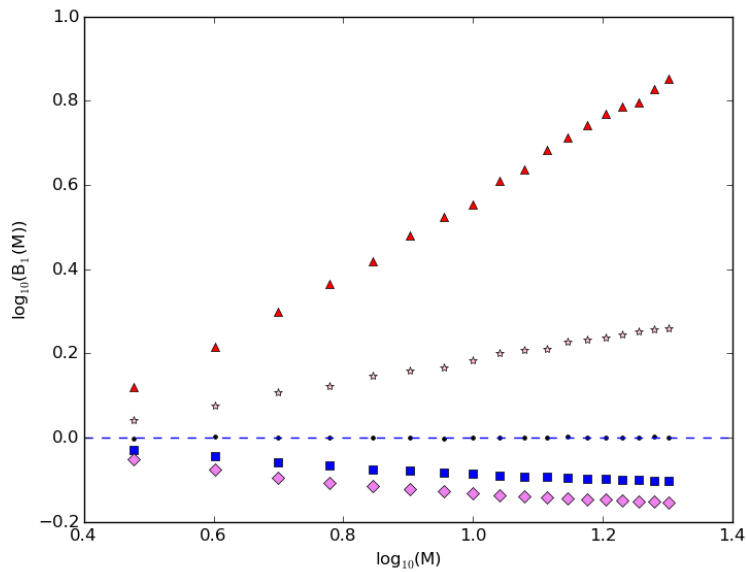


Figure 4 $B_1(M)$ against M for five noise spectra showing the ability to discriminate between different noise sources (white(dot), pink(star), red(triangles), blue(square), violet(diamond)).

All the above discussions regarding the different noise spectra have been based on a constant input signal. Given the fact that the Allan variance operates on small sections of data at a time there is, in fact, very little difference between the data shown in Figure 4 and what would be obtained if the data had underlying variations on a timescale larger than the value of M . An example of this is shown in Figure 5.

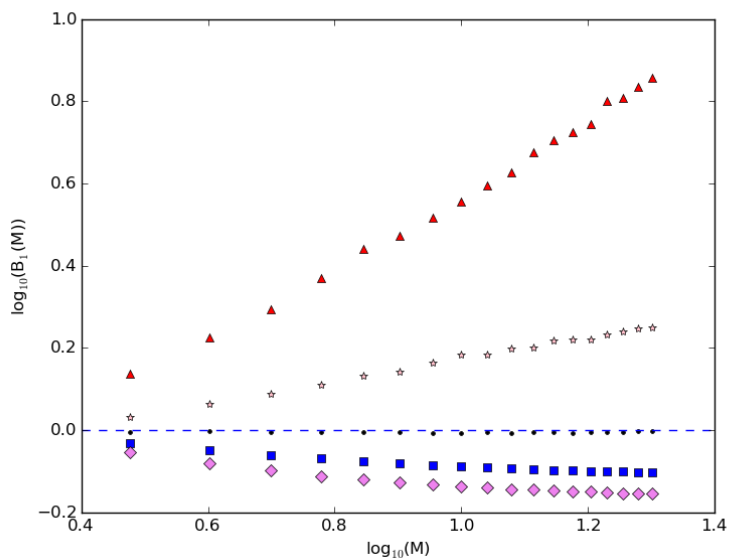


Figure 5 Same as Figure 4 where a sinusoid signal was added to the simulated data. The plot remains essentially unchanged from the constant signal case.

Instrument Noise characterization and the Allan/M-sample variance

4.2 Simulated data with gaps and with digitisation

4.2.1 Gaps in the data

The previous sections have been dealing with continuous simulated data. In reality, the data used for noise studies from many Earth observation satellites is not taken continuously but in little bursts. As an example, the AVHRR takes views of space in a burst of 10 measurements separated by approximately 6700 steps until another set of space measurements was taken. The same gap will be true of the internal calibration targets. While the literature on the Allan variance/M-sample variance has discussions on the issue of measurement dead time [2] this seems to be for the case where the dead time is distributed among the measurements which is not quite the case for an Earth observation satellite. We have therefore simulated a much longer time series and then only kept 10 measurements ignoring the next 6700 points and kept the next 10 measurements and so on. This has to be done to ensure that the power spectrum of noise is sampled correctly.

The same argument as was used regarding the impact of long timescale variations on the variances applies in this case as well, with the caveat that the range of M is limited to the continuously measured sections of data, which for the AVHRR restricts M to a range of 2-10. Care also has to be taken when calculating the M-sample variance with different values of M to make sure that only contiguous data is used and that the gaps are skipped over in the analysis. For cases where the value of M is significant compared to the length of a contiguous block this means that only one calculation of the statistic should be done before skipping to the next block of data. FN shows two $B_1(M)$ versus M plots for data with gaps where the gaps are ignored for the left hand plot and where the gaps are dealt with in the right hand plot. Note that the right hand plot looks just like the data from the continuous data shown in Figure 4 and Figure 5 whereas the left hand plot where the data across a gap is used is obviously different, especially for the red noise case. This then shows that even with large gaps between data the Allan variance/M-sample variance data can distinguish between different noise spectra as long as the gaps are dealt with appropriately.

Instrument Noise characterization and the Allan/M-sample variance

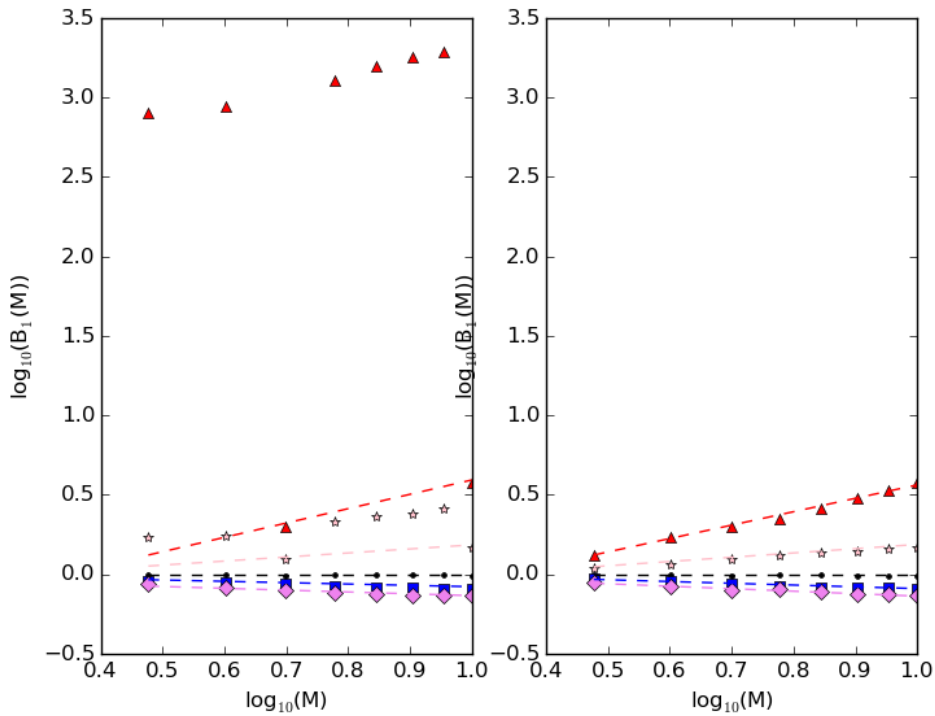


Figure 6 The left hand plot shows the $B_1(M)$ vs M data for data with gaps where the presence of gaps has been ignored in the analysis. The right hand plots shows the same data where gaps have been properly dealt with which gives very similar results to the continuous data cases shown in Section 4.1. Ignoring the presence of gaps in the data significantly impacts the pink and red noise data.

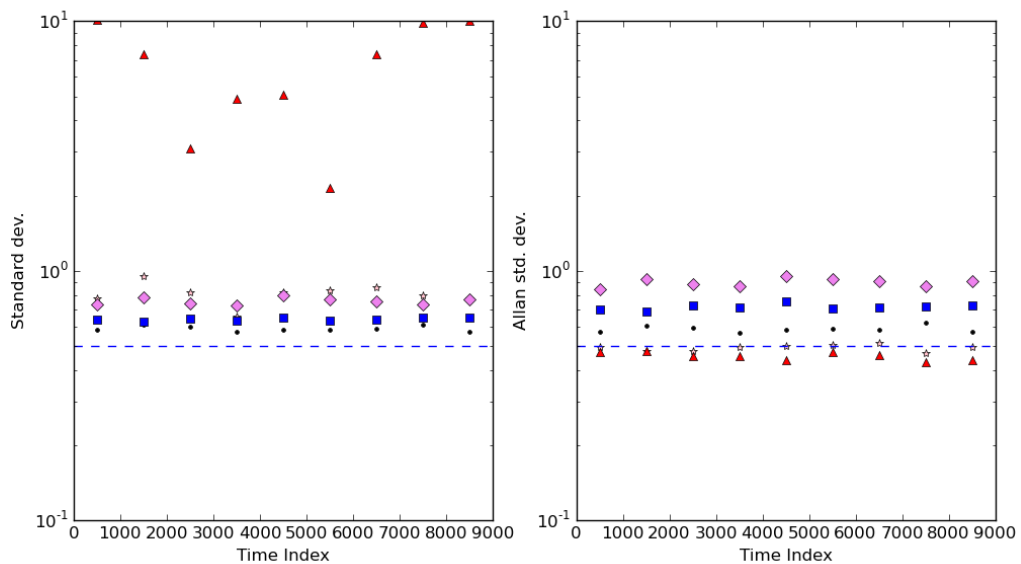


Figure 7 Same as Figure 3 but where digitisation has been applied. There is a shift caused when compared with Figure 3

Instrument Noise characterization and the Allan/M-sample variance

4.2.2 Effect of digitisation

All the above discussion has been made with simulated data where the input data has been floating point numbers. For Earth observation data from satellites this is rarely the case since the low level telemetry is always digitised. For heritage sensors this digitisation can be of the order of the underlying noise itself. As an example the AVHRR, which has a 10 bit digitisation, has detector noise that is of order 0.5 counts which means that the digitisation step is larger than the underlying noise value. Figure 7 shows similar data to that used in Figure 3 where the data has been digitised to integer counts before the Allan variance is calculated. There are distinct differences between Figure 7 and Figure 3 and in particular there is a shift to larger values. This represents what may be called ‘digitisation noise’ though it not strictly a noise component.

Figure 8 shows the $B_1(M)$ versus M case where digitisation has been included. Compared to Figure 4 it is clear that digitisation has had an impact on the $B_1(M)$ values where apart from the white noise case we always expect the $B_1(M)$ values to be one, the $B_1(M)$ values are suppressed relative to the non-digitised case. This means that if the $B_1(M)$ versus M relationship is to be used to determine the noise spectrum, the impact of digitisation has to be taken into account.

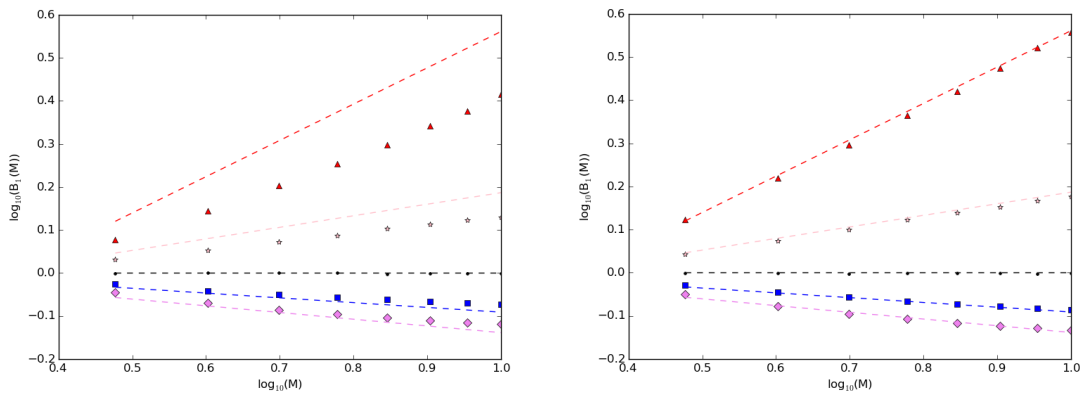


Figure 8 $B_1(M)$ against M including the effect of digitisation. The left hand plot is for a noise level of 0.5 counts and the right hand plot is for a noise level of 3 counts. Over plotted are the dependencies from Figure 4 and shows that digitisation changes the dependencies especially for the pink/red noise cases.

As the digitisation becomes less important (or the noise level in counts gets larger), the $B_1(M)$ versus M dependency gets close to the dependency where no digitisation is present. Figure 8 shows two examples. The left hand plot shows a highly digitised case where in input noise level is 0.5 counts and shows that the $B_1(M)$ versus M dependency is smaller than for the non-digitised case. The right hand plot shows a less heavily digitised case with a noise level of 3 counts. In this case the difference between the non-digitised and digitised values is small.

4.3 Analysis of data from the AVHRR

Sections 4.1 and 4.2 have shown the behaviour of the Allan variance and the M-sample variance for simulated data. Here we look at several examples taken from the AVHRR data record that include a range of different noise behaviour. TIROS-N shows bimodal noise within an orbit that has been ascribed to problems with the electronics, NOAA-07 shows large long term noise variations in the $3.7\mu\text{m}$ channel and NOAA-14 shows a more normal noise behaviour where the noise is approximately constant over time, at

Instrument Noise characterization and the Allan/M-sample variance

least until near the end of its operational life. The following sections show an Allan/M-sampling variance analysis for these three cases.

4.3.1 NOAA-14

To begin with we analyse 3 orbits of NOAA-14 AVHRR data from December 22nd 1997 looking at the 3.7 μ m and 11 μ m channels. Figure 9 shows the averaged count values over each 10 measurements (top panels) together with the standard deviations derived using the Allan variance on the 3.7 μ m channel data. The Allan variances have been averaged over 1000 scanlines or a time step of around 8 minutes. Note that the constant space view signal is due to an on-board electronic clamp system which sets the output voltage of the detector to zero when viewing space whereas the variable signal from the internal calibration target (ICT) view is due to instrument temperature changes around an orbit. The noise estimates from the Allan variance are shown in the lower two panels. They show an apparent periodic signal in the noise estimates of both the Space and ICT views which seems to be correlated with the raw ICT counts. Given that for the AVHRR a larger value of ICT counts means a smaller flux (note that the space view counts are at 992 counts) implies that a component of the noise is anti-correlated with the total flux hitting the detector. This is on the assumption that the total flux hitting the detector (a combination of instrument self-emission and the incoming signal) is directly related to the ICT temperature.

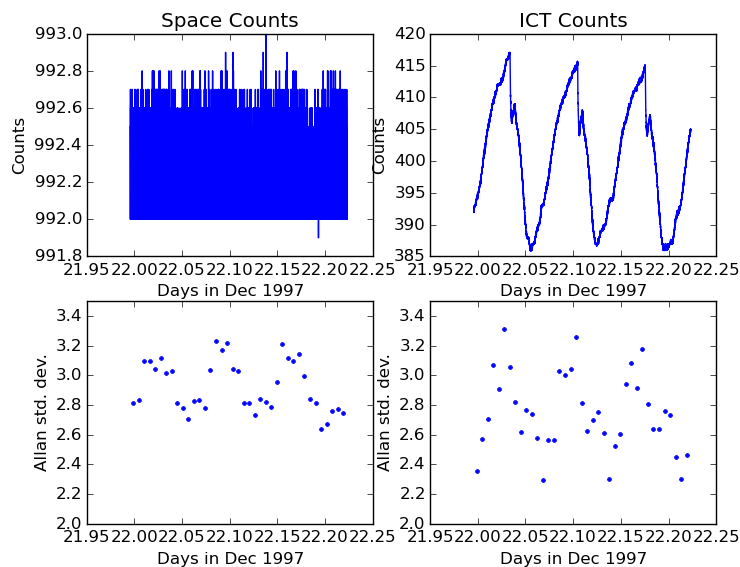


Figure 9 An Allan variance analysis for the 3.7 μ m channel taken from NOAA-14 in December 1997. The top two panels show the space counts and ICT counts averaged over a single observation. The lower two panels show the standard deviations derived from the Allan variance for the space and ICT views averaged over 1000 scanlines. IN both the Space view and ICT view data there is an apparent orbital variation.

For the 11 μ m channel it appears that there are distinct differences between the noise seen when viewing space and when viewing the internal calibration target (ICT) in that the noise seen for the space clamp seems larger than that seen when looking at the ICT (Figure 10). As with the 3.7 μ m channel there seems to be a hint of periodicity in the space count noise that looks like it has a small variation on orbital timescales.

To investigate the NOAA-14 noise signals further we have looked at the $B_1(M)$ versus M data. This is shown in Figure 11. For the 3.7 μ m channel the data seem consistent with a violet (proportional to the

Instrument Noise characterization and the Allan/M-sample variance

square of the frequency) noise spectrum whereas for the 11 μ m channel the closeness of the values to unity this indicates that white noise processes combined with some 1/f noise dominate the noise. Given that there is such a difference between the 3.7 μ m and 11 μ m channels it should be remembered that these two channels have different detectors and associated electronics which may help explain the difference in behaviour.

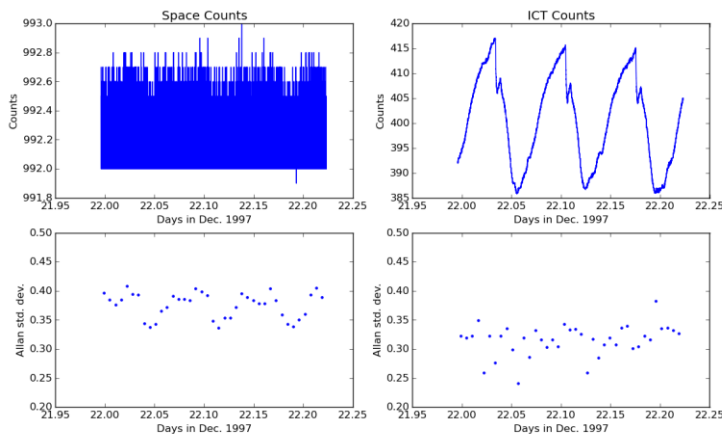


Figure 10 An Allan variance analysis for the 11 μ m channel for NOAA-14 done in a similar manner to the 3.7 μ m channel. Again there is evidence for an orbital variation in the Space view noise and it is also apparent that the noise values derived for the space and ICT view show a bias relative to each other.

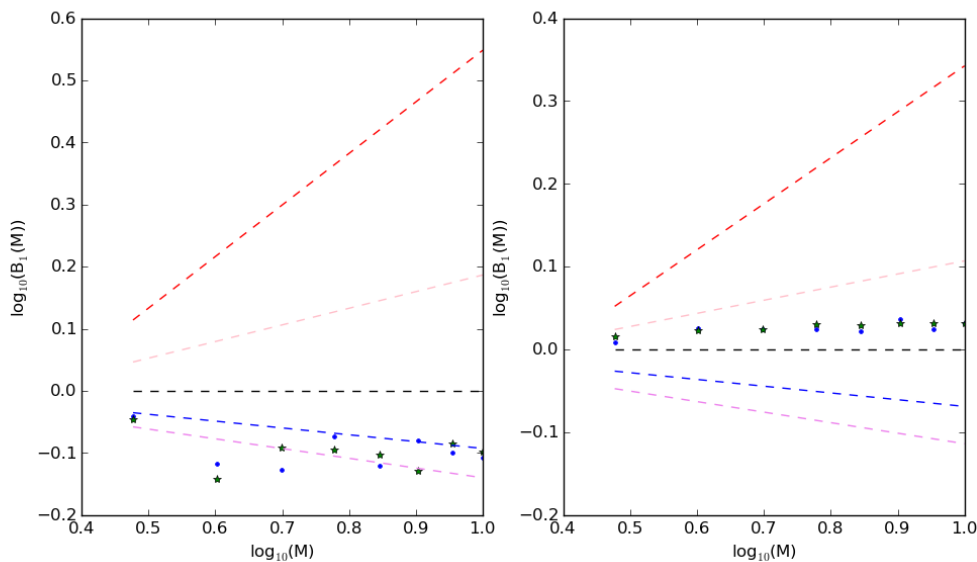


Figure 11 $B_1(M)$ against M for the NOAA-14 AVHRR data for both the space view (dots) and ICT views (crosses). The left hand plot is for the 3.7 μ m channel, the right hand plot is for the 11 μ m channel. The lines correspond to the dependencies from Figure 4. This indicates that for the 3.7 μ m channel violet noise is the closest match whereas white noise combined with some 1/f noise is the model for the 11 μ m channel.

4.3.2 TIROS-N

TIROS-N was the first of the AVHRR sensors (AVHRR/1) and was launched in 1978. It is known to have a significant noise problem in the 3.7 channel where at certain points in the orbit the noise is seen to

Instrument Noise characterization and the Allan/M-sample variance

dramatically increase which is thought to be due to pickup noise problems in the electronics and has not been seen in the later AVHRR sensors (the AVHRR/2 and AVHRR/3 sensors). This noise problem can be seen in Figure 12 which is derived in a similar manner to Figure 9 and Figure 10. In this case, however, the Allan variance has been calculated over a small averaging window (10 scan lines) to highlight the in-orbit variations in the noise. It can also be seen that the ICT noise during these increases is larger than the associated space view noise by approximately 50%.

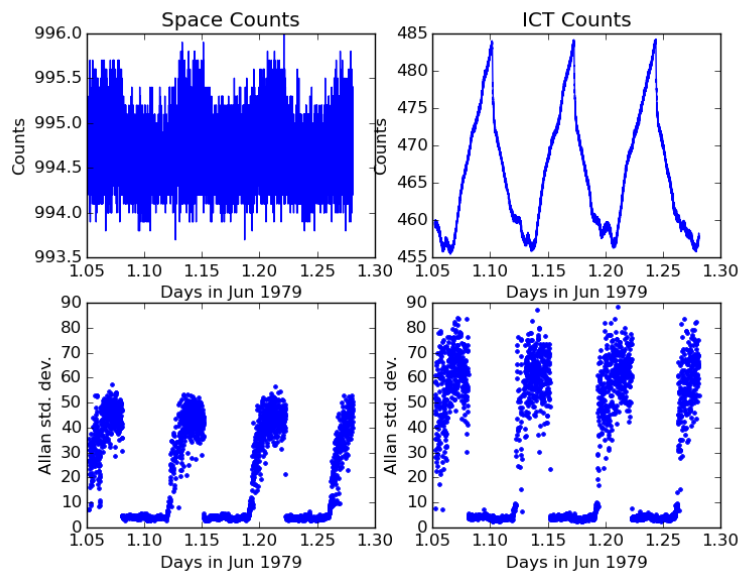


Figure 12 Noise characteristics for the 3.7 μ m channel from TIROS-N. Note the large systematic increase of noise at particular locations around the orbit.

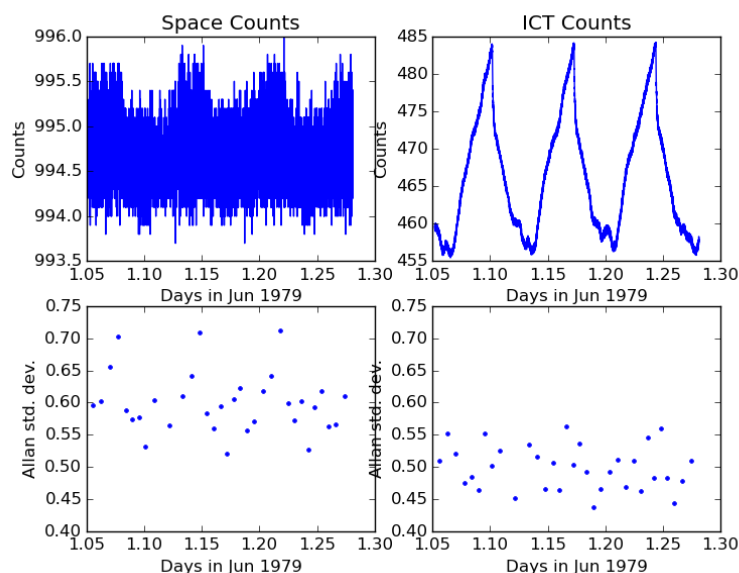


Figure 13 Noise data for the 11 μ m channel for TIROS-N. There is a similar orbital variation in the raw Space counts as was seen for the 3.7 μ m channel, but only marginal evidence for a period signal in the noise. As was seen in the NOAA-14 data there is also a shift to lower noise in the ICT data relative to the Space view data.

Instrument Noise characterization and the Allan/M-sample variance

The 11 μ m channel noise data is not as dramatic as the 3.7 μ m channel (see Figure 13). There is similar evidence for a periodic signal when compared to the NOAA-14 11 μ m channel and the data also shows a similar noise difference between the Space view and ICT views. Given that between TIROS-N and NOAA-14 there was approximately 18 years and a change in design it looks like the noise characteristics in the 11 μ m channel are remarkably similar.

As with NOAA-14 we can also look at the $B_1(M)$ versus M . This time, however, we separate out the two different noise regimes to see if there is any difference in the underlying noise spectrum. Note that while not clearly shown in Figure 12 the typical low noise value for TIROS-N of order 4 counts is similar to that seen for NOAA-14 where an average of 3.5 counts was seen. Using this threshold and separating out the two cases gives the data shown in Figure 14 for the 3.7 μ m channel and Figure 15 for the 11 μ m channel. As was the case for the 3.7 μ m channel of NOAA-14 the underlying noise looks like it has a higher dependency than one proportional to the frequency squared. The TIROS-N 11 μ m channel dependency is, however, completely different from that seen in NOAA-14 and does not seem to be consistent with a single source of noise.

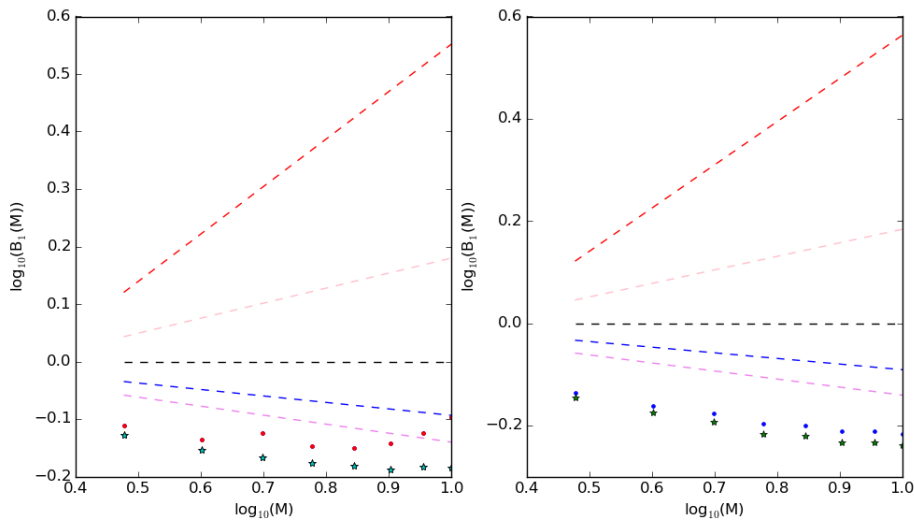


Figure 14 $B_1(M)$ against M for the TIROS-N 3.7 μ m channel data where the data has been split into times where the noise is low and high. Both the space view (dots) and the ICT view (stars) are shown. For both noise regime the inferred noise spectrum is greater than a proportional to frequency squared relation.

Instrument Noise characterization and the Allan/M-sample variance

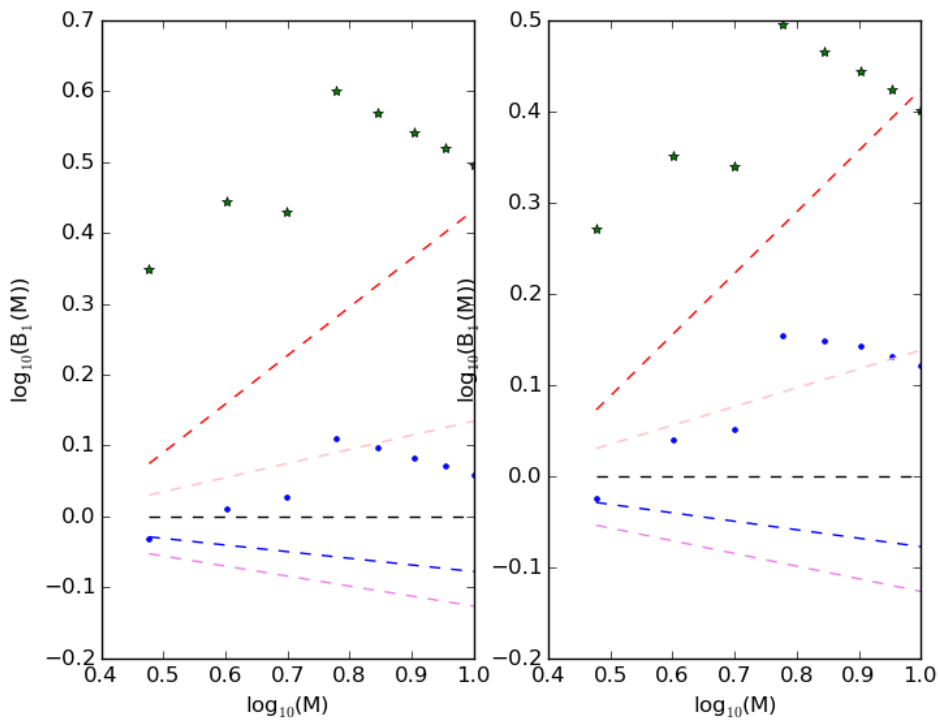


Figure 15 $B_1(M)$ against M for the $11\mu\text{m}$ channel of TIROS-N for the Space view (dots) and ICT view (stars) the two times used in Figure 14. Here the noise spectrum is very difficult to determine based on these plots.

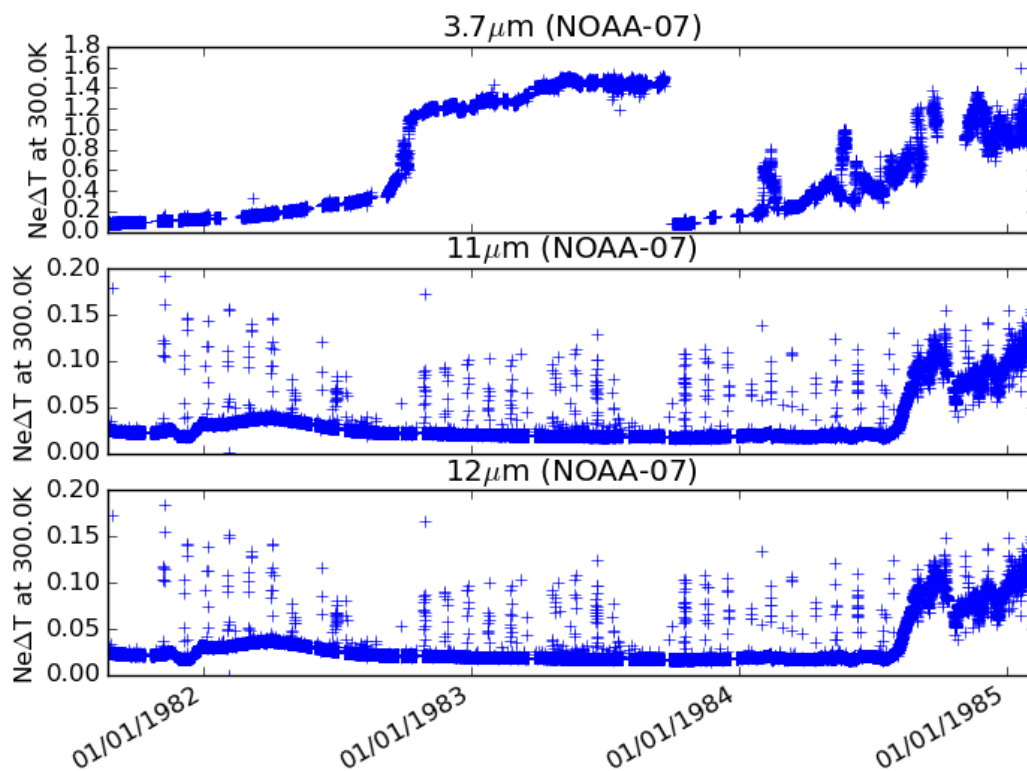


Figure 16 NeΔT for NOAA-07 over the sensor lifetime

Instrument Noise characterization and the Allan/M-sample variance

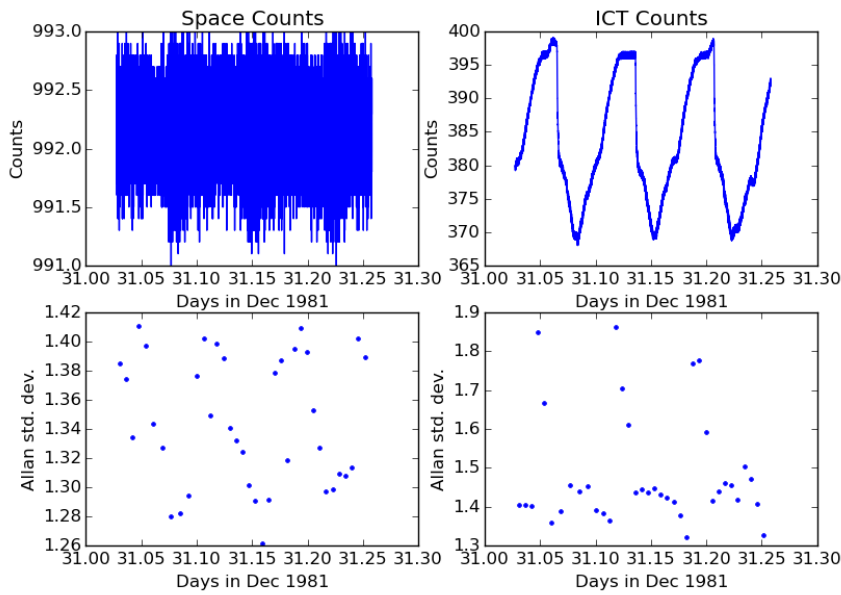


Figure 17 NOAA-07 data from 1981 for the 3.7 μ m channel

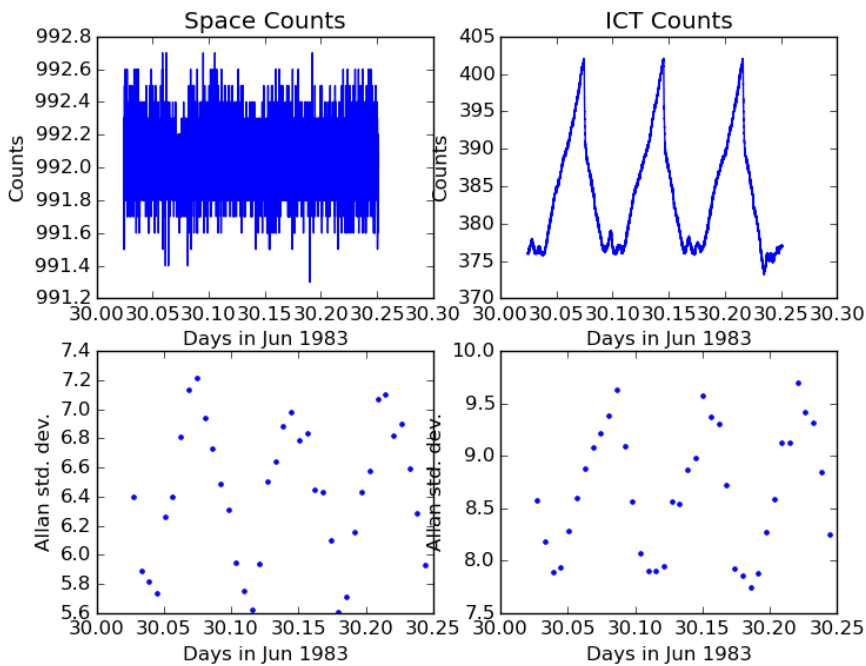


Figure 18 NOAA-07 data from 1983 for the 3.7 μ m channel

Instrument Noise characterization and the Allan/M-sample variance

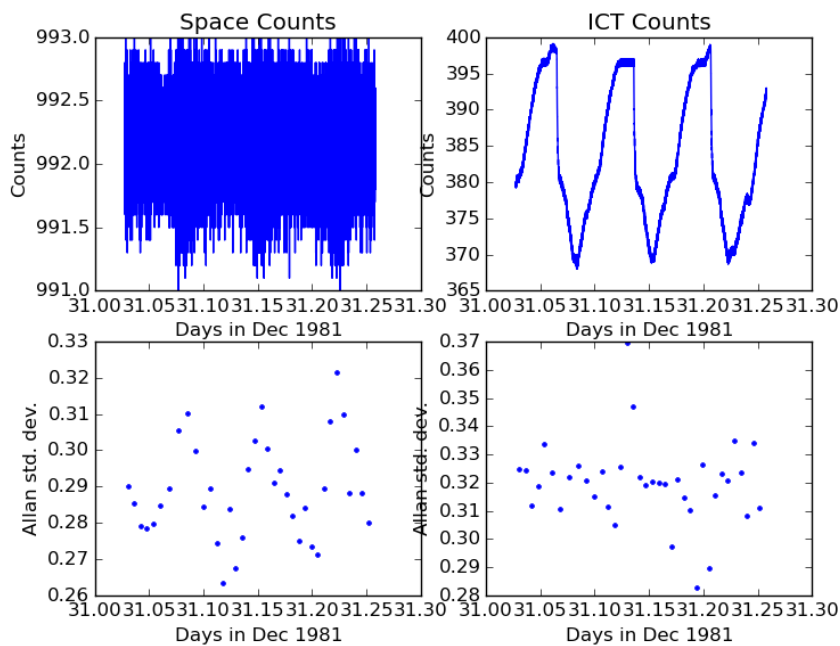


Figure 19 NOAA-07 data from 1981 for the 11 μ m channel

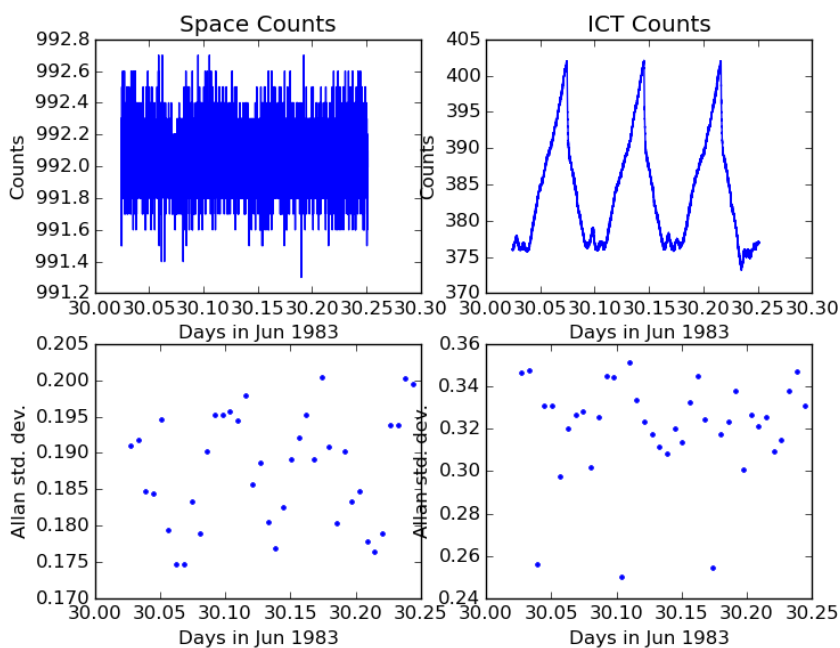


Figure 20 NOAA-07 data from 1983 for the 11 μ m channel

4.3.3 NOAA-07

Finally we have looks at two observation dates for NOAA-07 which cover the large change in noise seen over a long timescale. The strongest variation is seen in the 3.7 μ m channel and is shown in Figure 16. Note that in Figure 16 the Ne Δ T has been derived using standard techniques and does not use the Allan variance.

Instrument Noise characterization and the Allan/M-sample variance

The two selected dates (31/12/1981 and 30/06/1983) sample the low and high points of the noise. Noise plots are shown in Figure 17, Figure 18, Figure 19 and Figure 20 for the 3.7 μm and 11 μm channels and for a date in 1981 and 1983. For the 3.7 μm channel there are distinct differences between the 1981 and 1983 data. The 1981 data is similar in behaviour to that seen for NOAA-14 with a small period signal which is anti-correlated to the ICT signal. The ICT data does show some large deviation from the periodic signal which are likely due to solar contamination events. For the 11 μm channel the ICT noises are similar between then 1981 and 1983 data but while the Space view noise shows a strong periodic signal for both times, the 1983 Allan standard deviation is smaller than the 1981 case.

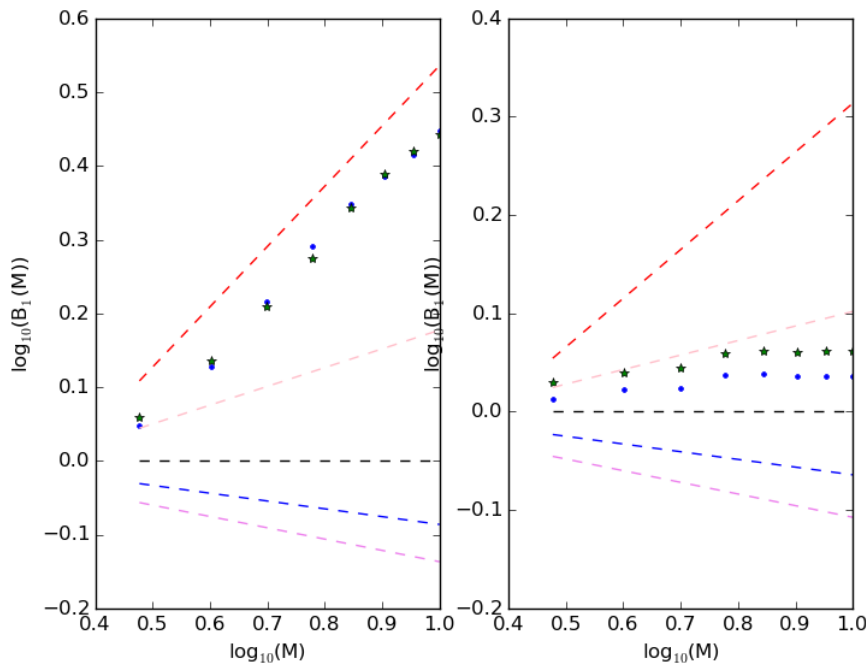


Figure 21 $B_1(M)$ against M for the 3.7 μm channel (left plot) and the 11 μm data (right plot) for 1981

In terms of the $B_1(M)$ versus M data unlike NOAA-14 and TIROS-N the noise spectrum for the 3.7 μm channel goes as f^2 rather than as $1/f^2$ and is consistently around the same noise spectrum for the two dates chosen (see Figure 21 and Figure 22). On the other hand the 11 μm channel dependency is similar to that seen for NOAA-14 which may imply a similar noise source for both.

4.3.4 Correlations between the noise and ICT radiance

Comparing the data between the sensors also show that there can be correlations between the Space view and the ICT radiance – in this case parameterised from the ICT counts which for the AVHRR are an inverted measure (low counts means more radiance). Note that we are essentially using the ICT radiance as a proxy for the instrument self-emission. Figure 23 shows some of the correlations and it can be seen that there is a consistent anti-correlation in the 3.7 μm channel for NOAA-07 and NOAA-14. The situation is less clear for the 11 μm channel where NOAA-07 shows a strong correlation between ICT radiance and noise but NOAA-14 does not. Such correlations are of interest as they may indicate a noise source. For example, a strong correlation between the noise and the ICT radiance could indicate that shot noise is important.

Instrument Noise characterization and the Allan/M-sample variance

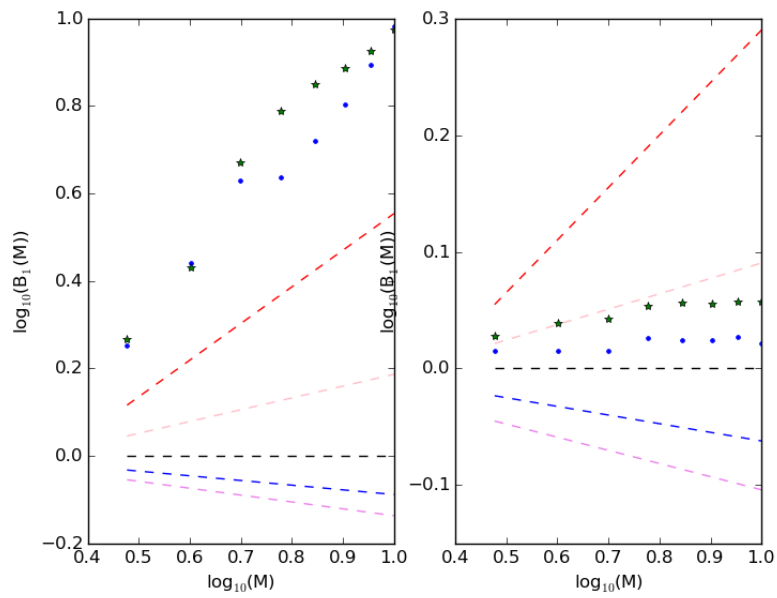
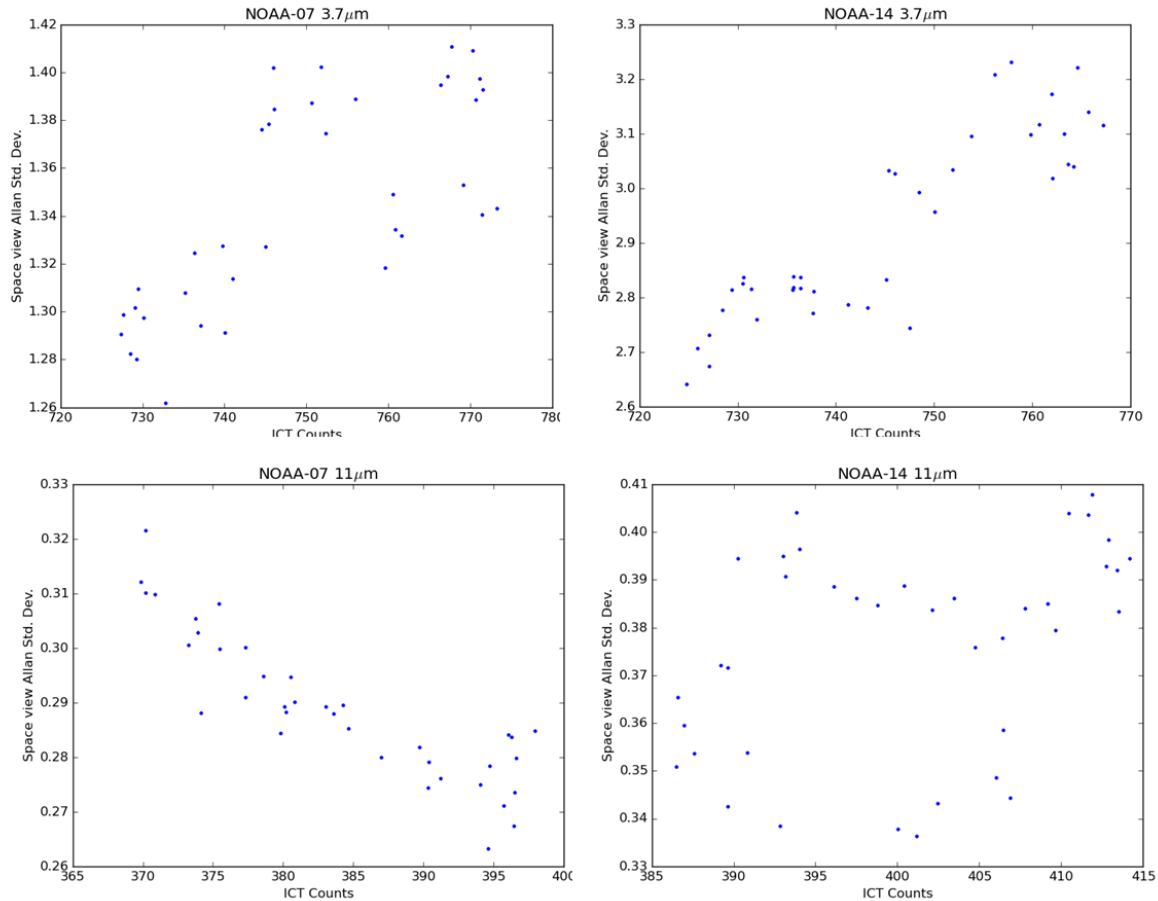


Figure 22 $B_1(M)$ against M for the $3.7\mu\text{m}$ channel (left plot) and the $11\mu\text{m}$ data (right plot) for 1983

Instrument Noise characterization and the Allan/M-sample variance

In this report we have introduced both the Allan variance along with the M-sample variance and through the use of simulations we have demonstrated that such statistics provide a robust means of estimating the underlying noise processes. This includes being able to determine which particular noise spectrum may



dominate. Real data from a number of AVHRRs has been used to demonstrate these techniques on real data and indicate a range of noise processes and correlations exist.

Figure 23 Correlations between the Space view Allan standard deviation and the ICT counts for NOAA-07 and NOAA-14

For example, across all three AVHRRs studied the 3.7μm channel was consistently a long way from white noise with NOAA-14 as $1/f^2$ whereas NOAA-07 as f^2 . For NOAA-07 and NOAA-14 the 11μm channel looks close to having a white (frequency independent) noise spectrum whereas the noise spectrum for TIROS-N is much more complex. For some channel/sensor combinations there is also evidence for correlations between proxies for the self-emission and the noise which indicates for at least one sensor/channel that shot noise may be important. A time line of the spectral slope could inform more about how the source of noise changes over time for all the channels.

In terms of analyses using within the FIDUCEO project the robustness of the Allan variance to non-stationary data (which is the case for many of the sensors within the project) as well as the extra information provided regarding the noise spectrum work indicate that the widespread use of these techniques should be recommended with the following caveats.

- Any gaps in the data should be correctly dealt with

Instrument Noise characterization and the Allan/M-sample variance

- $B_1(M)$ versus M analyses must take into account the impact of digitisation

The next step would be to extend this above analysis to complete time series for each sensor to see if the noise characteristics change over time. This would be greatly helped by the implementation of the Allan variance/M-sample variance as part of the FIDUCEO toolkit package.